Theor Chim Acta (1989) 75: 67-80

Theoretica Chimica Acta

Quantum theory of chemical bond formation processes in condensed systems: studies towards exploration of electrochemical dark and photoprocesses on semiconductors

C. Engler, E. Rabe, H. Schultz, and W. Lorenz

Sektion Chemie, Karl-Marx-Universität Leipzig, DDR-7010 Leipzig, German Democratic Republic

(Received February 15/Accepted March 22, 1988)

Quantum theoretical models of chemical bond formation and partial charge transfer processes in condensed systems, and their extension to processes in electronic non-equilibrium are investigated in this paper with a view to further exploration of electrochemical and photoelectrochemical kinetics on semiconductors. Electrochemical dark and photocurrents on n-III-V-semiconductors are correlated with calculated transition probabilities for atom-group transfer over larger distances (80 to 240 pm), leading to a first estimate of potential surface shapes compatible with experiment. Some specific problems connected with transition probability calculations for heavy-particle transfer in strong anharmonic potentials are considered in detail, including approximation of Franck-Condon transitions in arbitrary potentials by their classical limit.

Key words: Chemical bond formation — Condensed systems — Semiconducting — Electrochemical dark — Photoprocesses

1. Introduction

An important link between quantum chemical and electrochemical features of chemical elementary processes in condensed systems is brought about by the fact that electronic partial charge transfer is a ubiquitous quantum phenomenon connected with chemical bond breaking or bond formation. Joint consideration of chemical bond formation and charge transfer is particularly necessary in the study of interfacial electrochemical processes, where quantum-chemical partial charge transfer enters into macroscopic observables of electrical current flow.

Related topics are under development since the sixties and have been extended in recent years to semiconductor interfacial processes [1].

Quantum theoretical access to the dynamics of elementary chemical bond formation and partial charge transfer processes is provided by suitable treatment of the transition matrix [2]. Recent progress in this field includes the development of charge transfer kinetics in electronic non-equilibrium [1], which extends the applicability of quantumstatistical transition models to the fields of semiconductor electrochemistry and photoelectrochemistry.

In this paper, some problems related to these topics will be investigated. A short theoretical survey of quantum statistical Franck-Condon models and their application to chemical bond formation coupled with partial charge transfer, and of charge transfer kinetics in electronic non-equilibrium is given in Sect 2. Kinetic data characteristic of electrochemical dark and photoprocesses on n-III-V-semiconductors will be evaluated in Sect. 3. Calculations of species conversion probabilities will be covered in Sect. 4 for heavy-particle transfer in harmonic or anharmonic potentials over larger distances (approximately a bond length or a solvate radius) in different approximations, including quantum treatment of the reactive subsystem and classical treatment of the medium, or classical treatment of both (classical limit). The transition from quantal to classical regimes of kinetics, particularly with heavy-particle transfer in strong anharmonic potentials, is investigated more closely. Calculation data for kinetic charge injection coefficients (introduced in [1]) will be discussed in Sect. 5.

2. Theoretical survey

It may be illustrative to explain initially the peculiarities of partial charge transfer models using the example of electron exchange reactions in solution [3]. Electron exchange reactions are usually conceived as consisting of elementary steps with transfer of integral electrons. This picture does not take into account the partial charge transfer in chemical bonds between donor and acceptor atoms which comes into play with shorter donor-acceptor distance.

The essence of partial charge transfer models lies in the explicit inclusion into the theoretical framework of all chemical bonds within the donor-acceptor supermolecule. Electron delocalization is even allowed beyond the local, supermolecular reaction complex. Quantum theoretical analysis including the dynamics of the transfer process has been given in [2].

The development of dynamical partial charge transfer models was motivated by the fact that partial charge transfer of λ-type (the so-called quantum chemical or microscopic charge transfer which signifies the partial charge crossing a microscopic electrode interface in an elementary step) or of m-type (where the charge is injected into a semiconductor space charge layer) appears in the macroscopic charge balance of electrochemical processes [1a]. The quantum chemical approach of partial charge transfer in electrochemical systems, and the problems of distribution of partial charge transfer over the orbital energy scale, particularly in semiconductor interfacial processes, was discussed in [1c, 4].

2.1. *Transition matrix treatment of chemical bond formation and partial charge transfer processes*

Following a dynamical model treatment on the level of a Pauli master equation, we start with a transition probability expression

$$\langle P_{a\to b}\rangle = \frac{2\pi}{\hbar} Av\,|T_{ba}|^2 \cdot \delta(\Delta E^{\text{vib}} + \Delta E) \tag{1}$$

where Av denotes thermally weighted averaging of the initials and summation over final vibration states. T_{ba} are total transition matrix elements, ΔE^{vib} is the change of vibration energy in the conversion of $a \to b$, and ΔE is the total energy difference of the zero-points of initial (a) and final (b) state.

The transition matrix is in general defined in a diabatic representation of nuclear ($\phi_a\phi_b$) and electronic ($\varphi_a\varphi_b$) state vectors:

$$T_{ba} = \langle \phi_b | V | \phi_a \rangle; \qquad V = \langle \varphi_b | H^0 | \varphi_a \rangle \tag{2}$$

where V is the electronic transition element and H^0 is the (exact) hamiltonian in fixed-nuclei approximation. The eigenvectors of H^0 are adiabatic many-electron states. Adopting a 2-state model following [2, 5], we take into account the adiabatic ground-state vector $|\varphi_1\rangle$ and an excited state $|\varphi_2\rangle$, and of the corresponding adiabatic potential surfaces $E_1(R)$, $E_2(R)$ which depend on nuclear configuration. This full quantum theoretical procedure is capable of allowing for any chemical bond phenomena in the ground state of the system.

The diabatic electronic states appearing in (2) are obtained from $|\varphi_1\rangle$, $|\varphi_2\rangle$ by means of a unitary transformation

$$\begin{pmatrix} |\varphi_a\rangle \\ |\varphi_b\rangle \end{pmatrix} = U \cdot \begin{pmatrix} |\varphi_1\rangle \\ |\varphi_2\rangle \end{pmatrix}. \tag{3}$$

Eq. (3) leads to a nondiagonal representation of the hamiltonian, with diabatic electronic state vectors $|\varphi_a\rangle, |\varphi_b\rangle$ and related diabatic potential surfaces $E_a(R)$, $E_b(R)$ with respectively one minimum at position a or b, for which the nuclear state vectors $|\phi_a\rangle, |\phi_b\rangle$ are defined. The unitary 2-state matrix U takes the usual form

$$U = \begin{pmatrix} \sin x(R) & \cos x(R) \\ -\cos x(R) & \sin x(R) \end{pmatrix}$$

where $x(R)$ is a suitably chosen function of nuclear configuration. The electronic transition element V of Eq. (2) is then

$$V = \sin x(R) \cdot \cos x(R) \cdot [E_2(R) - E_1(R)] \tag{4}$$

which assumes a maximal value near $x(R^*) \simeq \pi/4$:

$$V_{\max} \simeq 0.5[E_2(R^*) - E_1(R^*)] \tag{4a}$$

R^* denotes a saddle point between the (adiabatic) ground state minima a and b. In the familiar Condon approximation, one gets

$$T_{ba} \simeq V_{\max} \cdot \langle \phi_b | \phi_a \rangle \tag{5}$$

where $\langle \varphi_b | \phi_a \rangle$ is the Franck–Condon overlap.

The extension of this transformation procedure to processes in condensed systems consisting of a reactive subsystem S and medium M has been treated in [2]. The possibility of partial charge transfer is guaranteed by this procedure due to the fact that near the minima of the transformed diabatic species potentials $E_a E_b$, the original adiabatic ground-state potential surface E_1 dominates; the latter gives full account of electron delocalization connected with chemical bonds [1, 2].

2.2. Quantum statistical Franck–Condon models

Once arrived at a diabatic potential surface representation, one can proceed with common Franck–Condon-type calculations. A well-justified approximation consists of a quantal representation of the reaction complex S and a classical (or high-temperature) representation of the medium M (cf. [6–9]). (1) in this case takes the form

$$\langle P_{a\to b}\rangle = \sum_v \sum_w P_{av\to bw}$$

$$= (\pi/\hbar^2 E_M kT)^{1/2} \cdot \left[\sum_v f(v)\right]^{-1} \cdot \sum_v \sum_w f(v) \cdot g(w, v) \tag{6}$$

with $f(v) = \exp \beta E_{aSv}$,

$$g(w, v) = |T^S_{bw,av}|^2 \cdot \exp \beta [E_{bSw} - E_{aSv} + E_M + \Delta E]^2 / 4E_M$$

$\beta = -1/kT$. E_M is the classical medium reorganization energy. The terms E_{aSv} and E_{bSw} are vibration levels of the reaction complex S in the initial (a) and final (b) state respectively v and w are quantum numbers. ΔE is the same as in Eq. (1); $T^S_{bw,av}$ are transition elements of the reaction complex S which have the form of Eqs. (2) or (5). In the following we shall occasionally compare harmonic and Morse potentials which are (in 1D) respectively

$$E(R) = E(R_0) + (k/2) \cdot (R - R_0)^2 \tag{7}$$

or

$$E(R) = E(R_0) + (k/2a^2) \cdot [1 - \exp(-a(R - R_0)]^2 \tag{8}$$

where R_0 corresponds to potential minimum, k is the harmonic force constant, and a the anharmonicity constant corresponding to a bond-dissociation energy $D = k/2a^2$.

Problems of dividing $\langle P\rangle$ into kinetic Arrhenius parameters, as well as quantum medium effects have been considered in [10]. Calculation of transition matrix elements $T^S_{bw,av}$ with Morse potentials up to higher vibration states v, w is available from [11a]; data for $\langle P\rangle$ and related quantities for harmonic and anharmonic potentials have been given in [9, 11].

With increasing reduced mass μ but otherwise fixed potential characteristics, the number of transition components $P_{av\to bw}$ to be allowed for in Eq. (6) increases rapidly and $\langle P\rangle$ ultimately goes to its classical limit for both the reactive subsystem S and medium M. Classical limits have been considered, e.g. in work on optical transitions [12], and are familiar in the above-mentioned reorganization energy concept [13] which is valid in harmonic approximation. A derivation of the classical limit of $\langle P\rangle$, valid for arbitrary potentials, has been made and the result

is briefly given in Appendix 1 of this paper; applications are included in the present study. The full classical regime of Franck-Condon transitions turns out to be most relevant for heavy-atom-group transfer in strong anharmonic potentials with low barrier height.

2.3. Charge transfer kinetics in electronic nonequilibrium

Semiconductor surface processes under current flow and/or illumination mostly proceed at strong electronic nonequilibrium. These conditions have been included in the transition matrix treatment, taking into account the partial charge injection into the medium (semiconductor space charge layer) accompanying an interfacial species conversion process, and also the electronic non-equilibrium of the medium. The theoretical argument is briefly as follows [1]. Charge injection is connected with energy injection which contributes to the term ΔE in Eq. (1). A compact expression can be given for the most relevant case of nondegenerate semiconductor relative to an electronic equilibrium reference state eq. For an electron injection process one obtains

$$\Delta E - \Delta E^{eq} = mkT \cdot \ln (n_s / n_s^0) \tag{9}$$

and for a hole injection process

$$\Delta E - \Delta E^{eq} = -mkT \cdot \ln (p_s / p_s^0) \tag{10}$$

where m is the charge (in units of elementary charge) injected in a forward process into the medium. n_s and p_s are the surface electron and hole densities (to be calculated from electronic balance and transport equations), and n_s^0 and p_s^0 their equilibrium values. Quantum statistical and thermodynamic suppositions connected with (9, 10) have been discussed in [1b] and [10].

Starting from Eqs. (9) and (10) for a conversion process of chemisorbed or physisorbed species A and B

$$A \underset{\nu_n}{\rightleftharpoons} B + mn^- \quad \text{or} \quad A + mp^+ \underset{\nu_p}{\rightleftharpoons} B \tag{11}$$

one gets the following kinetic equations for charge transfer in condensed systems:

$$\nu_n = \langle \vec{P}_n \rangle \cdot \Gamma_a - \langle \tilde{P}_n \rangle \cdot \Gamma_b; \qquad \nu_p = \langle \vec{P}_p \rangle \cdot \Gamma_a - \langle \tilde{P}_p \rangle \cdot \Gamma_b \tag{12}$$

with $\langle \vec{P}_n \rangle = \vec{\nu}_n \cdot (n_s)^{-\vec{m}}$, $\langle \tilde{P}_n \rangle = \tilde{\nu}_n \cdot (n_s)^{\tilde{m}}$

$$\langle \vec{P}_p \rangle = \vec{\nu}_p \cdot (p_s)^{\vec{m}}, \qquad \langle \tilde{P}_p \rangle = \tilde{\nu}_p \cdot (p_s)^{-\tilde{m}}. \tag{13}$$

In (12), Γ_a and Γ_b are adsorption densities of species A and B. The transition probabilities $\langle P \rangle$ are proportional to (i) the rate coefficients ν which depend mainly on the interfacial dipolar Helmholtz potential, and (ii) a fractional power of surface electron or hole density; $\vec{m}$ and $\tilde{m}$ are kinetic charge injection coefficients. The appearance of fractional electronic densities in both the forward and backward rate is a new feature which follows ultimately from microreversibility of the charge injection process.

2.4. Kinetic charge injection coefficients

The kinetic charge injection coefficients $\vec{m}$ and $\tilde{m}$ of Eqs. (13) are related to the injected charge m of Eqs. (11), according to

$$\vec{m} \approx m \cdot \partial \ln \langle \vec{P} \rangle / \beta \, \partial \Delta E, \qquad \tilde{m} \approx m \cdot \partial \ln \langle \tilde{P} \rangle / \beta \, \partial \Delta E \tag{14}$$

$\beta = -1/kT$. In Eq. (14), ΔE is referred to the initial state in both the forward and backward process. Small corrections to Eq. (14) have been given in [1b, 14]. The factors $\partial \ln \langle P \rangle / \beta \, \partial \Delta E$ are accessible by transition probability calculations and will be justified below in Sect. 5. They can usually be fitted sufficiently accurate by

$$\partial \ln \langle \vec{P} \rangle / \beta \, \partial \Delta E = \vec{a} + \vec{b} \cdot \Delta E + \vec{c} \cdot (\Delta E)^2 \tag{15}$$

and similarly $\partial \ln \langle \overleftarrow{P} \rangle / \beta \partial \Delta E$. According to Eqs. (9) and (10), the position of ΔE is somewhat different for non-equilibrium processes with electrons or holes (corresponding to dark or photoprocesses on n-semiconductors). One gets (cf. [14])

$$\vec{a} + \overleftarrow{a} = 1, \qquad \vec{b} = \overleftarrow{b}, \qquad \vec{c} = -\overleftarrow{c}. \tag{16}$$

Possible distortion of potential surface shape under ΔE-variation will at first be neglected.

2.5. Discussion

Little is known so far about chemical bond breaking and formation processes in strongly interacting reaction complexes with atom-group transfer over larger distances ΔR between initial and final potential minimum. For a process connected with interchange of sites within the solvate shell, one can estimate ΔR to be of the order of magnitude of a bond length or of a solvate radius, from structural arguments and (with increasing reliability) from quantum chemical data. In Sect. 4 we therefore start with a proof of Franck–Condon transitions for atom or atom-group transfer in the range 80 to 240 pm.

Charge transfer depends on electron delocalization and can take place over much larger distance (>1000 pm, cf. e.g. [15, 16]), when the electronic matrix element V_{max} remains sufficiently large at large donor-acceptor distance. Decrease of V_{max} according to Eq. (4a) is generally expected with decreasing donor-acceptor interaction.

3. Kinetic data of electrochemical dark and photodissolution of *n*-III-V-semiconductors

As a second input for evaluation, we estimate in this section a possible order of magnitude of transition probability $\langle P \rangle$ for the primary step of electrochemical n-III-V- semiconductor dissolution. On n-GaAs or n-GaP, stationary anodic dark or photocurrents due to semiconductor dissolution lie in the range

$$j^{dark} \simeq 10 \text{ to } 10^2 \text{ nAcm}^{-2}; \qquad j^{photo} \simeq \text{mAcm}^{-2}. \tag{17}$$

The dark current on n-materials is an electron current, the photocurrent a hole current. Independently of detailed mechanism, we can presume a reaction sequence with consecutive reaction steps. With the stationarity condition required for a sequence, $\bar{v}_1 = \bar{v}_2 = \cdots \bar{v}_i$, and the stationary current is

$$\bar{j} = \sum m_i f \bar{v}_i = (\sum m_i) F \bar{v}_1 = z F \bar{v}_1 \tag{18}$$

where z is the overall charge number of the electrochemical process. For a totally

irreversible anodic process sequence [17] one gets from (12): $\bar{v}_1 = \langle \vec{P}_1 \rangle \cdot \Gamma_a$. This scheme is to be expected when an AB semiconductor is dissolved by direct transfer of oxidized A and B in turn into the solution, and may likewise be possible when dissolution proceeds over intermediate crystallographic positions at the interface (cf. discussion in [18]). With $z = 6$ to 8 and a rough estimate of an upper limit of density of dissolution sites of $\Gamma_a < 10^{-11}$ mol cm^{-2} (or $< 10^{-2}$ of a monolayer), one obtains for the primary, controlling semiconductor dissolution step from Eqs. (17) and (18)

$$\langle \vec{P}_n \rangle_{\text{dark}} > 10^{-3}\text{–}10^{-2}\ \text{s}^{-1}. \qquad \langle \vec{P}_p \rangle_{\text{photo}} > 10^{2}\ \text{s}^{-1}. \tag{19}$$

This lower-limit estimate of $\langle \vec{P} \rangle$ points to a medium-sized activation barrier.

This estimate also holds roughly when near-equilibrium steps precede the irreversible, controlling step, because the density of the intermediate which reacts in the controlling forward process is then in equilibrium with dissolution sites and can hardly exceed the estimated density Γ_a.

The injected partial charge m appearing in Eqs (9)–(11) can be expected to be either in the range about 2–4 for direct transfer of oxidized A and B into solution, or to be smaller when the dissolution proceeds over intermediate positions on the surface.

4. Transition probabilities for heavy particle transfer over larger distance: discussion of problems and some first results

Exploration of local potential surfaces for chemical species conversion processes on semiconductor interfaces is still in its infancy. In advance of potential surface data, particularly for the type of processes addressed in the preceding section, we attempt here to get some information about possible potential surface shapes compatible with both the expected potential minima distance ΔR considered in Sect. 2.5, and the order of magnitude of transition probabilities $\langle P \rangle$ estimated in Sect. 3. For that purpose we limit ourselves, in first approximation, to a 1-dimensional reaction path model which we consider in its transformed diabatic representation.

As a rule, a sufficiently large $\langle P \rangle$ at large ΔR is realized when both the electronic transition element and the Franck-Condon overlap are relatively large (a not too large medium reorganization energy of the semiclassical model, Eq. (6) is also required). The former condition is mostly obeyed at strong chemisorption (estimated $V_{\max} \gg 10^{-1}$ eV); the latter condition requires flat potentials in the vibration overlap region of initial and final state. Anharmonicity of potential surfaces thus plays a decisive role in large-distance transfer.

Another point already addressed in Sect. 2.2, concerns the importance of the classical limit of $\langle P \rangle$ in heavy-particle transfer. In this limit the potential surface shapes are the sole quantities controlling the transition probability. Some representative data determined using the formulas briefly outlined in Appendix 1 are given in Sect. 4.4. In this connection, the transition from the quantal treatment

of the reactive subsystem S into its classical limit requires further investigation: preliminary data is given in Sect. 4.3. Some properties of the quantumstatistical Franck-Condon representation following Eq. (6) are briefly considered once more in Appendix 2.

4.1. Estimate of adiabatic potentials by inverse transformation of diabatic model potentials

Transformation of the original adiabatic state vectors and potentials into diabatic ones is determined by the unitary matrix U given in Eq. (3). In advance of detailed knowledge of adiabatic potentials E_1 E_2 which appear in Eqs. (4) and (4a), it is reasonable to first pursue a reverse procedure and invert Eq. (3) in order to get information about adiabatic potentials which are compatible with kinetically adjusted diabatic model potentials. Some tentative estimates, particularly with diabatic potentials of anharmonic Morse type, are under further development.

4.2. A representative example of heavy-particle transfer in strong anharmonic potentials over large distance

An example of flat anharmonic potentials in the vibration overlap range which simulates some qualitative features of a bond dissociation process on a semiconductor interface coupled with simultaneous solvation bond formation, is shown in Fig. 1 (quantitative assignment is not intended at the present stage). Transition probabilities $\langle P \rangle$ in these potentials, calculated in the classical limit, are given in Table 1.

The classical limit is usually a lower bound of quantum statistical calculation (for exceptions see Sect. 4.3). The results of Table 1 therefore demonstrate the general possibility of relatively large transition probabilities under the condition

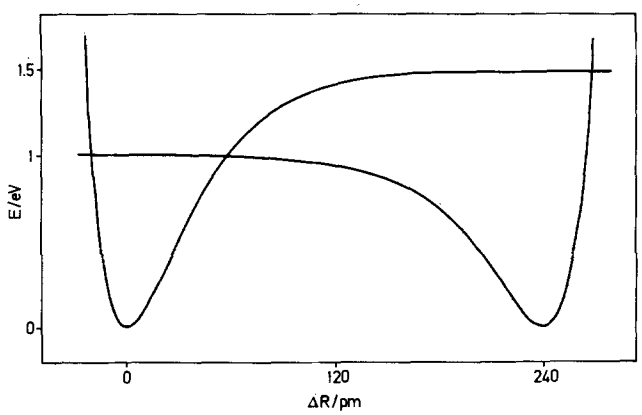

Fig. 1. Example of anharmonic diabatic potential curves for the initial and final state. Morse potentials with harmonic force constants $k_a = 4.1 \cdot 10^2\ \mathrm{Nm^{-1}}$ (or $\mathrm{kg\,s^{-2}}$), $k_b = 2.8 \cdot 10^2\ \mathrm{Nm^{-1}}$, anharmonicity constants $a_a = 29.4\ (\mathrm{nm})^{-1}$, $a_b = -29.4\ (\mathrm{nm})^{-1}$ (corresponding to bond dissociation energies $D_a =$ 1.5 eV, $D_b = 1.0$ eV), $\Delta R = 240$ pm, $\Delta E = 0$

of large potential minima distance $\Delta R \simeq 240$ pm. This is true even at $\Delta E \simeq 0$ where the barrier is almost 1 eV.

The latter value for the barrier is likewise representative for a forward transition probability $\langle \vec{P} \rangle$ of equal magnitude as given in Table 1, but at $\Delta E < 0$. Figure 1 shows a least favourable case in so far as $\langle \vec{P} \rangle$ is large (this does not exclude kinetic irreversibility, since the backward rate $\langle \vec{P} \rangle \cdot \Gamma_b$ can be negligible when, in chemical non-equilibrium Γ_b is small). The same forward transition probability $\langle \vec{P} \rangle$ as in Table 1 but a much lower backward transition probability $\langle \tilde{P} \rangle$ is obtained when, at fixed potential curve shape near the diabatic intersection, ΔE is made <0 by lowering the potential minimum b (right-hand minimum in Fig. 1).

4.3. Transition from quantal to classical regime of heavy-particle transfer

An estimate of the validity of the classical limit of chemical species conversion probabilities can be obtained by investigating the transition from the quantal to the classical regime of the reactive process in the subsystem *S*. To that end we have started a closer comparison of the quantum statistical model using Eq. (6), and its classical limit using Eq. (A2) or (A3) of Appendix 1.

Some results are given in Table 2 which refer to examples with relatively small force constants and low barriers. For such cases the following statements can be made:

(a) For transitions using Morse potentials, the classical limit provides a very good approximation of $\langle P \rangle$ even at small reduced mass μ, being better with smaller ΔR values.

(b) At fixed force constants k and potential minima distance ΔR, and fixed reduced mass μ in the quantum cases, one observes a much larger ratio $\langle P \rangle_{\text{quantal}} / \langle P \rangle_{\text{classical}}$ with harmonic than with Morse potentials, mainly due to the larger barrier in the former cases.

Within the framework of Eq. (6), the relation

$$\ln \langle \vec{P} \rangle / \langle \tilde{P} \rangle = \ln (Z_b / Z_a) + \beta \Delta E \tag{20}$$

holds for any potential [9]. Z_a and Z_b are the vibration partition functions of the initial and final state. Eq. (20) allows to prove that in the summation over v and w in Eq. (6) all relevant terms have been allowed for.

In the last columns of Table 2 are given the expansion parameters a, b, c of Eq. (15). They will be discussed in Sect. 5. Equations (16) provide another proof of numerical consistency.

Table 1. Classical limit of transition probabilities $\langle P \rangle$ for the strong anharmonic potentials shown in Fig. 1. T 300 K, $\beta = -38{,}65\ \text{eV}^{-1}$, E_M 1 eV, $V_{\max}$ 1 eV. $\langle P \rangle$ calculated from Eq. (A2)

ΔE/eV	−0.5	−0.25	0	+0.25	+0.5
$\langle \vec{P} \rangle / \text{s}^{-1}$	$1.2 \cdot 10^{7}$	$6.4 \cdot 10^{3}$	1.2	$9.8 \cdot 10^{-5}$	$1.3 \cdot 10^{-8}$
$\langle \tilde{P} \rangle / \text{s}^{-1}$	$4.1 \cdot 10^{-2}$	$3.3 \cdot 10^{-1}$	0.95	1.2	2.5

Table 2. Transition probability parameters in Eqs. (6) or (A2), and (15). T 300 K, E_M 2 eV, V_{max} 1 eV, k_a 16.6 Nm^{-1} (or $kg\,s^{-2}$), k_b 66.4 Nm^{-1}, a_a 8 $(nm)^{-1}$, a_b −16 $(nm)^{-1}$. Harmonic frequencies: at μ 1 $g\,mol^{-1}$: ω_a $1 \cdot 10^{14}\,s^{-1}$, ω_b $2 \cdot 10^{14}\,s^{-1}$, at μ 30 $g\,mol^{-1}$: ω_a $1.8 \cdot 10^{13}\,s^{-1}$, ω_b $3.7 \cdot 10^{13}\,s^{-1}$

ΔR/pm		$\ln\langle\tilde{P}\rangle$	$\ln\langle\tilde{P}\rangle$ at $\Delta E = 0$	$\tilde{a}$	$\tilde{a}$	$\tilde{b} = \bar{b}$ eV^{-1}	$\tilde{c} = -\bar{c}$ eV^{-2}
80	harmonic, $\mu = 1$	12.6	13.9	0.48	0.52	0.22	0.01
	harmonic, classical	11.9	12.6	0.47	0.53	0.21	0.01
	Morse, $\mu = 1$	14.6	15.9	0.49	0.51	0.23	0.01
	Morse, $\mu = 30$	14.3	15.0	0.48	0.52	0.22	0.02
	Morse, classical	14.3	15.0	0.48	0.52	0.22	0.02
120	harmonic, $\mu = 1$	7.1	8.4	0.46	0.54	0.19	0.01
	harmonic, classical	5.1	5.8	0.44	0.56	0.17	0.02
	Morse, $\mu = 1$	12.1	13.4	0.47	0.53	0.20	0.035
	Morse, classical	11.7	12.4	0.46	0.54	0.19	0.05
160	harmonic, $\mu = 1$	−0.8	0.5	0.43	0.57	0.16	0.01
	harmonic, classical	−4.7	−4.0	0.41	0.59	0.13	0.02
	Morse, $\mu = 1$	9.6	10.9	0.45	0.55	0.16	0.08
	Morse, classical	9.1	9.8	0.43	0.57	0.15	0.10

Usually the quantumstatistical treatment yields larger transition probabilities than those calculated in the classical limit. There are however exceptions: one can get $\langle P\rangle_{quantal} < \langle P\rangle_{classical}$ when, in the quantal case with small reduced mass and large vibration quantum $\hbar\omega$, a transition component from vibration ground state into one final state dominates strongly, while the classical limit corresponds to reduced mass $\mu \to \infty$ with (in principle) an infinite number of transition components.

Another peculiarity occurs in very flat anharmonic potentials, again with small reduced mass μ and large vibration quantum $\hbar\omega$, when transition components near the Morse dissociation limit have not yet reached the maximum of the probability distribution of transition components (see Fig. 2 in Appendix 2) or have only slightly fallen short of the maximum. In such cases (partly observed in Fig. 1) the Morse potential approximation itself requires reconsideration, so far as the supposed reduced mass is relevant. Further calculations related to these points will be reported when they have been completed.

5. Kinetic charge injection coefficients

For mechanistic decision it is desirable to have a theoretical estimate of the ratio of the kinetic charge injection coefficients $\vec{m}$ or $\bar{m}$ to the injected charge m, which according to Eq. (14) is mediated by the factor

$$\partial \ln\langle P\rangle/\beta\,\partial\Delta E \tag{21}$$

Table 3. Kinetic charge injection parameters for the anharmonic example of Fig. 1 and Table 1, $\tilde{a}$ 0.95, $\tilde{a}$ 0.05, $\tilde{b} = \bar{b} = -0.20\,eV^{-1}$, $\tilde{c} = -\bar{c} = -0.94\,eV^{-2}$

ΔE/eV	−0.5	−0..25	0	+0.25	+0.5
$\partial \ln\langle\vec{P}\rangle/\beta\partial\Delta E$	0.82	0.94	0.95	0.84	0.62
$\partial \ln\langle\bar{P}\rangle/\beta\partial\Delta E$	0.18	0.06	0.05	0.16	0.38

Eq. (21) takes the value 0.5 in harmonic potentials with equal force constants in the initial and final state at $\Delta E = 0$. Generally one can deduce some influence of the slope of the initial and final potential curves at their intersection, by consideration of the classical forward and backward activation barriers well-known since early electrochemical kinetics (usually applied to Helmholtz potential shifts on metal electrodes). Derivation of Eq. (21) from $\langle P \rangle$ calculations takes into account further dynamical factors and therefore gives a more definite proof.

The examples of Table 2 show only moderate deviations of Eq. (21) from 0.5 as is seen in the parameters a, b, c of Eq. (15). A quite different result is obtained with the potential curves of Fig. 1: data for Eq. (21) given in Table 3 point out very asymmetric values for the forward and backward processes thus confirming the qualitative influence of different potential curve slopes at the intersection. Calculation of Eq. (21) includes all additional controlling factors which gain influence (particularly in the regime of Eq. (6)).

A quantum effect in the semiclassical model of Eq. (6), which could give rise to oscillatory ΔE-dependence of kinetic charge injection coefficient $\vec{m}$ or $\tilde{m}$, can usually be ruled out in electrochemical systems with fluid electrolyte. This is confirmed in Appendix 3.

6. Summary

This paper treats some problems of the quantum theory of chemical elementary processes in condensed systems, with a view to exploring chemical bond formation and partial charge transfer in electrochemical dark and photoprocesses on semiconductors. This work prepares for the kinetic evaluation of local potential surfaces, and provides information about the following points:

Calculation of transition probabilities for heavy-particle transfer over large distances (80 to 240 pm) in strong anharmonic potentials.

Study of the transition from quantal to classical regime of heavy-particle transfer over low or medium-sized barriers, and application of the classical limit of Franck–Condon transitions in arbitrary potentials.

Calculation data concerning the ratio of the kinetic charge injection coefficients $\vec{m}$ and $\tilde{m}$ appearing in kinetic equations for charge transfer processes in electronic non-equilibrium, to the partial charge m injected in the elementary process into the semiconductor space charge layer, which essentially depends on potential surface shapes.

Appendix 1: The classical limit of Franck–Condon transitions in arbitrary potentials

Referring to Sects. 2.2 and 4, we briefly outline here the classical limit of Franck–Condon transitions in arbitrary potentials. Vibration levels E_{av} and E_{bw} in this limit become continuous functions of the transfer coordinate R, i.e.

$E_{av} \to E_a(R)$, $E_{bw} \to E_b(R)$, where E_a and E_b are the initial and final potential curves. For a 1D-system without medium, one gets in the Condon approximation

$$\langle P \rangle = \frac{2\pi}{\hbar} \cdot V_{\max}^2 \cdot (Z_a^{cl})^{-1} \cdot (|de/dR|_{R_s})^{-1} \cdot \exp \beta E_a(R_s) \tag{A1}$$

where Z_a^{cl} is the classical vibration partition function of initial states, $e(R) = [E_b(R) - E_a(R) + \Delta E]$, and R_s is the solution of $e(R) = 0$. Eq. (A1) holds for arbitrary potentials $E_a E_b$. For harmonic potentials with equal initial and final force constant, one gets from Eq. (A1) the familiar reorganization energy formula of [13].

For a system composed of a classical anharmonic reactive subsystem S and harmonic medium M, one gets

$$\langle P \rangle = (\pi/\hbar^2 E_m kT)^{1/2} \cdot V_{\max}^2 \cdot (Z_a^{cl})^{-1} \cdot \int_{-\infty}^{+\infty} dR \cdot \exp \beta e^*(R) \tag{A2}$$

where $e^*(R) = E_a(R) + [E_b(R) - E_a(R) + E_M + \Delta E]^2/4E_M$ and Z_a^{cl} refers to the reactive subsystem S. Solving the integral in Eq. (A2) by means of the saddle point method (which is exact with harmonic potentials and a good approximation for not too large anharmonicities and not too large potential maxima distances ΔR), one gets

$$\langle P \rangle = (\pi/\hbar^2 E_M kT)^{1/2} \cdot V_{\max}^2 \cdot k_a^{1/2} \cdot (\partial^2 e^*/\partial R^2)_{R_s}^{-1/2} \cdot \exp \beta e^*(R_s) \tag{A3}$$

where k_a is the force constant of the initial potential curve of the subsystem S, and R_s the solution of $(\partial e^*/\partial R) = 0$. In examples like that of Fig. 1, direct evaluation of Eq. (A2) is preferable.

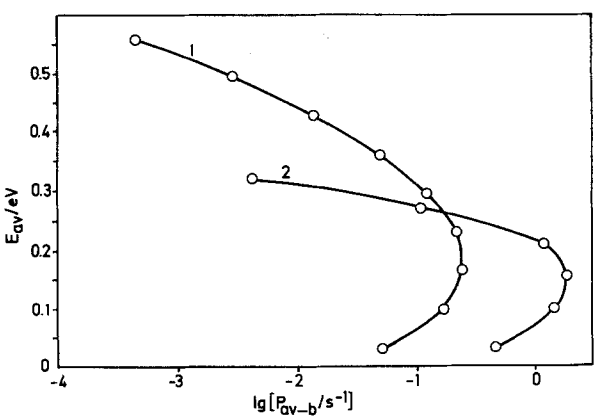

Fig. 2. Distribution of thermally weighted transition components $P_{av \to b}$ from Eq. (6) and (A4) over initial vibration energy, *Curve 1:* harmonic potentials; *curve 2:* Morse potentials. $T = 300$ K, $E_M = 2$ eV, $V_{\max} = 0.3$ eV, $\Delta E = +0.5$ eV, $\mu = 1$ g mol^{-1}, $\Delta R = 80$ pm, force constants $k_a = 16.6$ Nm^{-1}, $k_b = 66.4$ Nm^{-1}, anharmonicity constants $a_a = 8$ (nm)$^{-1}$, $a_b = -16$ (nm)$^{-1}$, harmonic frequencies $\omega_a = 1 \cdot 10^{14}$ s^{-1}, $\omega_b = 2 \cdot 10^{14}$ s^{-1}

Appendix 2: Distribution of transition components over initial vibration energy

Detailed information about the transition process is contained in the distribution of thermally weighted transition components in the model of Eq. (6),

$$P_{av\to b} \equiv \sum_w P_{av\to bw} \tag{A4}$$

over initial vibration states (v). For given force constants k and reduced mass, Morse-P-values usually exceed harmonic ones by several orders of magnitude particularly at larger potential minima distance; cf. [2a, 9] and Table 2 of this paper. $P_{av\to b}$ runs with increasing v through a maximum, due to competition of decreasing Boltzmann factor $f(v)$ and initially increasing factor $\sum_w g(w, v)$. At larger v, Morse transition distributions can occassionally fall off steeply: Fig. 2 shows an example where this feature is particularly pronounced.

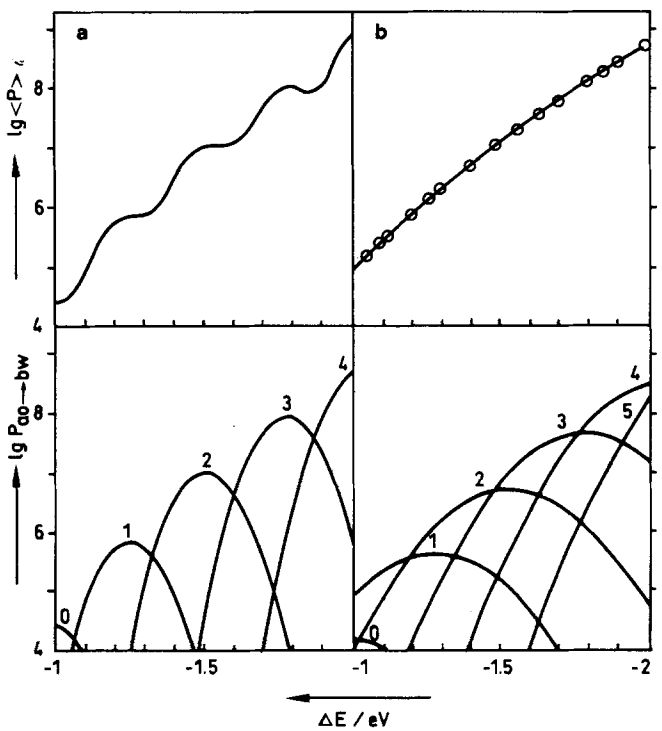

Fig. 3a, b. Range of appearance of quantum oscillations in the ln $\langle P\rangle - \Delta E$ – relation of Eq. (6). *Top*: total transition probability $\langle P\rangle$; *bottom*: transition components $P_{a0\to bw}$ (quantum number w labelled on the curves). **a** $T = 30$ K (narrow Gauss curves $P_{a0\to bw}$, leading to quantum oscillations in $\langle P\rangle$). **b** $T = 120$ K (broader Gauss curves $P_{a0\to bw}$, leading to suppression of oscillations; also at 60 K). $E_M = 1$ eV, $\omega_a = \omega_b = 3.9 \cdot 10^{14}\ s^{-1}$. The appearance of quantum oscillations does not critically depend on the transition matrix elements $T^S_{bw,a0}$. For simplicity harmonic potentials with $k_a = k_b = 250\ Nm^{-1}$ and ΔR 100 pm have been chosen

Appendix 3: Quantum effects in the semiclassical ln $\langle P\rangle - \Delta E$ relation.

The semiclassical transition probability $\langle P\rangle$ of Eq. (6) at low temperatures can exhibit an oscillating dependence on ΔE. The range of appearance of this quantum effect is of interest since it could in turn exert influence upon the kinetic charge injection coefficienents $\vec{m}$ and $\overleftarrow{m}$, which are proportional to $\partial \ln \langle P\rangle / \beta \partial \Delta E$.

The following discussion supports that these quantum oscillations are confined to temperatures far below room temperature as already pointed out in [8]. Let us first suppose that transitions from initial vibration state $v=0$ are favoured, which is the case when $\hbar\omega_a$ is at least >5 kT. Further we limit ourselves to $\omega_a = \omega_b = \omega$. Then oscillations in ln $\langle P\rangle$ over ΔE occur, when $(\Delta E + E_M) < 0$, and at the most two terms $g(w, 0)$ in Eq. (6) contribute at given ΔE significantly to $\sum_w g(w, 0)$. The latter condition requires $g(w, 0)$ to be narrow Gauss curves over ΔE, obeying

$$\hbar\omega \geqslant 4(E_M kT)^{1/2} \quad \text{(condition for quantum oscillations).} \tag{A5}$$

Figure 3 shows two examples, one with and the other without quantum oscillations in ln $\langle P\rangle$ over ΔE. Weaker exothermicity with $(\Delta E + E_M) \gtrsim 0$, or more than on relevant vibration mode in the quantum subsystem leads to strong suppression of the quantum oscillations.

References

1. Lorenz W (1985) J Electroanal Chem Interfacial Electrochem 191:31; (1986) Z Phys Chem 267:673; (1987) Phys Stat Sol (b) 144:585
2. Lorenz W, Engler C (1984) Phys Stat Sol (b) 122:745; Lorenz W (1982) Z Phys Chem 263:433; Engler C (1984) Z Phys Chem 265:513
3. Newton MD, Sutin N (1984) Ann Rev Phys Chem 35:437
4. Lorenz W, Katterle T (1987) Phys Stat Sol (b) 142:149
5. Schatz GC, Ross J (1977) J Chem Phys 66:1021; Mukamel S, Ross J (1977) J Chem Phys 66:3759
6. Dogonadze RR, Kuznetsov AM, Vorotyntsev MA (1972) Phys Stat Sol (b) 54:125
7. Kestner NR, Logan J, Jortner J (1974) J Phys Chem 78:2148
8. Ulstrup J, Jortner J (1975) J Chem Phys 63:4358
9. Engler C, Lorenz W (1984) J Electroanal Chem Interfacial Electrochem 171:123
10. Lorenz W, Engler C (1986) J Electroanal Chem Interfacial Electrochem 204:13
11. Engler C (1984) Z Phys Chem 265:1193; Engler C, Wiegratz S (1986) Z Phys Chem 267:365; Engler C, Rabe E (1986) Phys Stat Sol (b) 138:477
12. Lax M (1952) J Chem Phys 20:1752
13. Marcus R A (1956) J Chem Phys 24:966
14. Aegerter C, Lorenz W (1986) J Electroanal Chem Interfacial Electrochem 209:259
15. Larsson S (1983) J Chem Soc Faraday Trans, 2 79:1375
16. Heitele H, Michel-Bayerle M E, Finckh P (1987) Chem Phys Lett 134:237
17. Lorenz W, Wolf B (1983) Electrochim Acta 28:191; 1255
18. Lorenz W, Aegerter C, Handschuh M (1987) J Electroanal Chem Interfacial Electrochem 221:33